

# Magnetite/Ceria-Codecorated Titanoniobate Nanosheet: A 2D Catalytic Nanoprobe for Efficient Enrichment and Programmed Dephosphorylation of Phosphopeptides

Qianhao Min,<sup>†,‡</sup> Siyuan Li,<sup>†,‡</sup> Xueqin Chen,<sup>†</sup> E. S. Abdel-Halim,<sup>§</sup> Li-Ping Jiang,<sup>\*,†</sup> and Jun-Jie Zhu<sup>\*,†</sup>

<sup>†</sup>State Key Laboratory of Analytical Chemistry for Life Science, School of Chemistry and Chemical Engineering, Nanjing University, Nanjing 210093, P. R. China

<sup>§</sup>Petrochemical Research Chair, Chemistry Department, College of Science, King Saud University, P.O. Box 2455, Riyadh 11451, Saudi Arabia

## Supporting Information

**ABSTRACT:** Global characterization and in-depth understanding of phosphoproteome based on mass spectrometry (MS) desperately needs a highly efficient affinity probe during sample preparation. In this work, a ternary nanocomposite of magnetite/ceria-codecorated titanoniobate nanosheet (MC-TiNbNS) was synthesized by the electrostatic assembly of  $\text{Fe}_3\text{O}_4$  nanospheres and *in situ* growth of  $\text{CeO}_2$  nanoparticles on pre-exfoliated titanoniobate and eventually utilized as the probe and catalyst for the enrichment and dephosphorylation of phosphopeptides. The two-dimensional (2D) structured titanoniobate nanosheet not only promoted the efficacy of capturing phosphopeptides with enlarged surface area, but also functioned as a substrate for embracing the magnetic anchor  $\text{Fe}_3\text{O}_4$  to enable magnetic separation and mimic phosphatase  $\text{CeO}_2$  to produce identifying signatures of phosphopeptides. Compared to single-component TiNbNS or  $\text{CeO}_2$  nanoparticles, the ternary nanocomposite provided direct evidence of the number of phosphorylation sites while maintaining the enrichment efficiency. Moreover, by altering the on-sheet  $\text{CeO}_2$  coverage, the dephosphorylation activity could be fine-tuned, generating continuously adjustable signal intensities of both phosphopeptides and their dephosphorylated tags. Exhaustive detection of both mono- and multiphosphorylated peptides with precise counting of their phosphorylation sites was achieved in the primary mass spectra in the cases of digests of standard phosphoprotein and skim milk, as well as a more complex biological sample, human serum. With the resulting highly informative mass spectra, this multifunctional probe can be used as a promising tool for the fast and comprehensive characterization of phosphopeptides in MS-based phosphoproteomics.

**KEYWORDS:** 2D nanosheet, ternary nanocomposite, phosphopeptide, enrichment, dephosphorylation



## INTRODUCTION

As a fundamental post-translational modification occurring widely in biological entities, reversible protein phosphorylation is an essential pathway for the implementation of protein functionality and the regulation of enzyme activity.<sup>1</sup> Nevertheless, for a long time, in-depth and comprehensive characterization of protein phosphorylation was always restricted by the low abundance and high dynamic range of phosphorylated proteins and peptides, even by mass spectrometry (MS), the premier means for current proteome research.<sup>2–5</sup> To tackle this challenge, picking the target phosphorylated species out of high-complexity biomolecules has been accomplished by the principles of immobilized metal ion affinity chromatography (IMAC)<sup>6–8</sup> and metal oxide affinity chromatography (MOAC).<sup>9,10</sup> Rather than IMAC strategies involving possible metal-ion leakage, a wide diversity of elaborately structured transition-metal oxides (such as  $\text{TiO}_2$ ,<sup>9,11,12</sup>  $\text{ZrO}_2$ ,<sup>10,13</sup>  $\text{Al}_2\text{O}_3$ ,<sup>14,15</sup>  $\text{Nb}_2\text{O}_5$ ,<sup>16</sup> and  $\text{SnO}_2$ <sup>17,18</sup>) were alternatively developed as probes with excellent selectivity and recovery,

due to the robust Lewis acid–base interaction with phosphate moieties. To maximize the separation efficiency for phosphopeptides, enormous efforts have recently been made to explore mesoporous structured MOAC affinity probes, such as mesoporous  $\text{TiO}_2$ ,<sup>19</sup>  $\text{ZrO}_2$ ,<sup>20</sup> and  $\text{SnO}_2$ ,<sup>21</sup> mesoporous silica-supported nanocomposites;<sup>22,23</sup> and magnetic core–mesoporous shell architectures,<sup>24,25</sup> because of their extremely high surface areas and excellent surface properties. At the same time, considering the rapid isolation and high recovery rate of magnetic particles with the aid of an external magnetic field, further functionalizing the above metal oxides with magnetites in a core–shell fashion has become a prevailing mode for devising separation probes.<sup>26,27</sup>

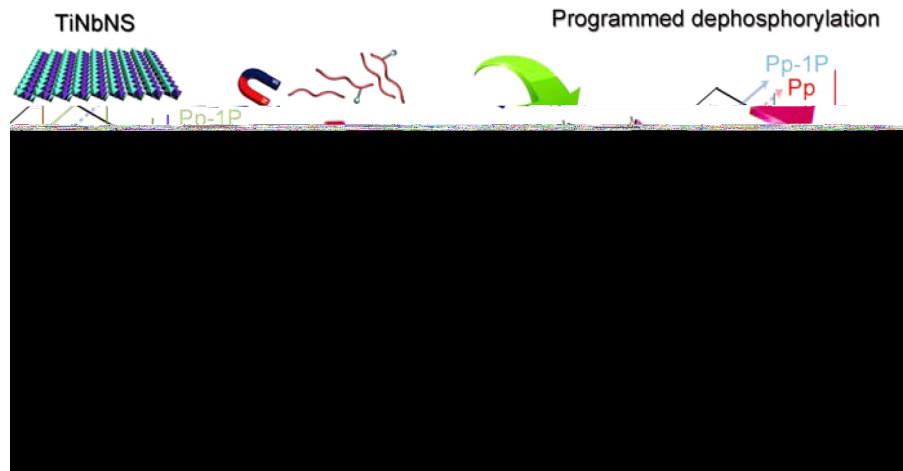
In the universe of phosphate affinity nanoprobes,  $\text{CeO}_2$  is a unique type that was recently employed as the “solid

Received: February 3, 2015

Accepted: March 25, 2015

Published: March 25, 2015

**Scheme 1.** Schematic Diagram of the Synthetic Strategy for MC-TiNbNS Composite and the Mechanism of Phosphopeptide Enrichment and Dephosphorylation



phosphatase” that efficiently mediated the dephosphorylation of phosphopeptides,<sup>28,29</sup> facilitating the identification of phosphopeptides by the mass difference of 80 Da between adjacent peaks. This natural advantage avoids the tedious procedure of conventional tandem mass spectrometry (MS2) analysis to verify phosphopeptides and realized direct recognition at the level of primary mass spectrometry (MS1). Such functionalities have also been demonstrated for other rare earth compounds including REPO<sub>4</sub> (RE = Eu, Tb, Er, Yb, Gd, Y) and GdF<sub>3</sub>.<sup>30–32</sup> However, existing CeO<sub>2</sub>-containing or lanthanide materials were synthesized with fixed compositions, surface components, and morphologies, yielding a constant hydrolytic catalytic activity in a given case.<sup>24,33</sup> With regard to the high dynamic range of phosphorylation, it was difficult to observe every dephosphorylated state for all of the phosphopeptides in a certain specimen, particularly for low-abundance or multiphosphorylated peptides, which suffer from low ionization efficiency. Moreover, despite the capability for dephosphorylation, the performance of existing CeO<sub>2</sub> or lanthanide nanostructures (focused on nanoparticles, nanospheres, and core–shell architectures) in harvesting phosphopeptides has yet to be improved, compared with diversely structured (mesoporous<sup>19,25,34</sup> and silica<sup>35,36</sup>/graphene-supported<sup>37–39</sup>) TiO<sub>2</sub> and ZrO<sub>2</sub> materials and derivate composites with maximized enrichment efficiency.

Two-dimensional (2D) materials including graphene, transition-metal dichalcogenides (TMDs), and transition-metal oxides (TMOs) present a wide variety of intriguing properties in sensing, catalysis, and energy transduction because of its 2D structural systems,<sup>21,40–44</sup> while also having great application potential in biological separation. Graphene initially underscored this promising possibility by acting as the scaffold to support metal ions or oxides for enhancing phosphopeptide enrichment,<sup>45–48</sup> giving us inspiration for offsetting the deficiencies of CeO<sub>2</sub> materials in the global characterization of phosphopeptides. Very recently, we employed another 2D nanomaterial, titanoniobate nanosheet (TiNbNS), composed of TiO<sub>6</sub> and NbO<sub>6</sub> octahedra and exfoliated from the layered metal oxide HTiNbO<sub>5</sub>, to form an Fe<sub>3</sub>O<sub>4</sub> nanocrystal-embedded nanocomposite for highly efficient capture of phosphopeptides.<sup>49</sup>

Herein, we further extended the ability of the 2D phosphate absorbent TiNbNS to construct a ternary nanocomposite of

magnetite/ceria-codedecorated titanoniobate nanosheet (MC-TiNbNS). As illustrated in Scheme 1, this 2D nanoprobe was generated by a two-step protocol, including preloading of Fe<sub>3</sub>O<sub>4</sub> nanospheres by electrostatic interaction and in situ growth of CeO<sub>2</sub> nanoparticles from Ce<sup>3+</sup> in the presence of hexamethylenetetramine (HMT). In this composite, TiNbNS serves not only as a platform for simultaneously holding CeO<sub>2</sub> and Fe<sub>3</sub>O<sub>4</sub> nanoparticles but also as a 2D adsorbent of phosphopeptides, compensating for the relatively low efficiency of CeO<sub>2</sub> nanoparticles; Fe<sub>3</sub>O<sub>4</sub> nanospheres endow the entire composite with a magnetic response, speeding and facilitating sample preparation; and the central role played by CeO<sub>2</sub> is to produce a set of dephosphorylated signatures for each phosphopeptide. Taking advantage of spacious reactive surface of 2D TiNbNS, the coverage of the CeO<sub>2</sub> component can be elaborately regulated to achieve simultaneous enrichment and programmed dephosphorylation of phosphopeptides, thus providing identifying information on phosphopeptides and an exact count of phosphorylation sites.

## EXPERIMENTAL SECTION

**Chemicals and Materials.** Trifluoroacetic acid (TFA), poly-(diallyldimethylammonium chloride) (PDDA) solution (20%), 4-nitrophenyl phosphate di(tris) salt (pNPP), 2,5-dihydroxybenzoic acid (DHB), trypsin (from bovine pancreas, TPCK treated),  $\beta$ -casein (from bovine milk), and bovine serum albumin (BSA) were all purchased from Sigma (St. Louis, MO). Iron(III) chloride hexahydrate ( $\text{FeCl}_3 \cdot 6\text{H}_2\text{O}$ ), 1,6-hexanediamine, anhydrous sodium acetate ( $\text{CH}_3\text{COONa}$ ), ammonium bicarbonate ( $\text{NH}_4\text{HCO}_3$ ), cerium(III) nitrate hexahydrate [ $\text{Ce}(\text{NO}_3)_3 \cdot 6\text{H}_2\text{O}$ ], titanium(IV) oxide ( $\text{TiO}_2$ ), niobium(V) oxide ( $\text{Nb}_2\text{O}_5$ ), potassium carbonate ( $\text{K}_2\text{CO}_3$ ), urea, and 10% tetrabutylammonium hydroxide (TBAH) were obtained from Shanghai Reagent Co. (Shanghai, China). Hexamethylenetetramine (HMT) was purchased from Shanghai Shunqiang Reagent Co. (Shanghai, China). Acetonitrile (ACN) of chromatographic grade was obtained from Merck (Darmstadt, Germany), and all other chemicals including nitric acid ( $\text{HNO}_3$ ) and ammonium hydroxide ( $\text{NH}_3 \cdot \text{H}_2\text{O}$ ) were of analytical grade.

**Preparation of Titanoniobate Nanosheets,  $\text{Fe}_3\text{O}_4$  Nanospheres, and MC-TiNbNS Composite.** First, KTiNbO<sub>5</sub> was prepared by heating a stoichiometric mixture of Nb<sub>2</sub>O<sub>5</sub>, K<sub>2</sub>CO<sub>3</sub>, and TiO<sub>2</sub> in a tube furnace at 1100 °C for 24 h at a heating rate at 5 °C/min. The protonated form, HTiNbO<sub>5</sub>, was synthesized by continuous stirring of a KTiNbO<sub>5</sub> suspension in 2 M HNO<sub>3</sub> at 70 °C for 6 h to accomplish cation exchange. The obtained HTiNbO<sub>5</sub> particles were

washed with distilled water and dried in air at 60 °C overnight. To prepare titanoniobate nanosheets (TiNbNS), 1 g of HTiNbO<sub>5</sub> was dispersed in 100 mL of distilled water, and then 10 wt % TBAH solution was slowly introduced until the pH value reached 10, after which the mixture was stirred continuously at room temperature for 7 days. Finally, incompletely exfoliated bulk materials were removed from the suspensions by centrifugation at 9000 rpm for 8 min, and the supernatant colloids containing the exfoliated nanosheets were kept for further use.

Fe<sub>3</sub>O<sub>4</sub> nanospheres were generated by a microwave solvothermal reaction. One gram of FeCl<sub>3</sub>·6H<sub>2</sub>O, 2 g of anhydrous sodium acetate, and 6.5 g of 1,6-hexamidine were successively dissolved in 30 mL of ethylene glycol with stirring for 15 min until transparency. The precursor solution was then transferred into a microwave synthesis system and reacted at 200 °C for 30 min (45 psi upon stability). After the microwave solvothermal reaction, the product magnetites were collected and washed with ethanol and water twice with the help of an external magnet. Ten milligrams of as-synthesized Fe<sub>3</sub>O<sub>4</sub> nanoparticles was redispersed in 0.5% PDDA aqueous solution and shaken for 20 min. Then, PDDA-coated Fe<sub>3</sub>O<sub>4</sub> microspheres were recovered with an external magnet and rinsed with water three times.

Magnetite-attached TiNbNS was obtained by mixing a 0.9 mL portion of an Fe<sub>3</sub>O<sub>4</sub> suspension (10 mg/mL) with 5 mL of TiNbNS (12.5 mg/mL) colloid in 30 mL of ethanol and vibrated at a vortex for 30 min. After that, a given amount of Ce(NO<sub>3</sub>)<sub>3</sub>·6H<sub>2</sub>O was added to the solution with ultrasonic vibration for 15 min. Subsequently, a corresponding amount of HMT initially dissolved in 15 mL of deionized water was added and treated with ultrasonic vibration for another 15 min. The fully dispersed particle solution was then mechanically stirred in an oil bath maintained at 70 °C for 2 h. Finally, magnetite/ceria-codedecorated TiNbNS (MC-TiNbNS) was magnetically separated, washed with deionized water and ethanol, and lyophilized to dryness. As a control, pure CeO<sub>2</sub> nanoparticles were prepared by the identical method in the absence of Fe<sub>3</sub>O<sub>4</sub> nanospheres and TiNbNS.

**Hydrolysis of Phosphate Ester by MC-TiNbNS.** A stock solution of *p*-nitrophenylphosphate (pNPP) (650 μmol/L) was prepared in 10% NH<sub>3</sub>·H<sub>2</sub>O in advance. Then, 20 μL of pNPP solution was mixed with 20 μL of the suspension of MC-TiNbNS composite (10 mg/mL) and sonicated at room temperature for 3–60 min. Water in the sonicator was refreshed every 10 min to keep the temperature constant. At a given reaction time, the resulting solution was rapidly isolated from MC-TiNbNS solids with the help of a magnet, and 10 μL of the supernatant was pipetted for UV-vis spectroscopy characterization. The concentration of reactant pNPP and product pNP were monitored by the UV absorbance at  $\lambda = 310$  and 401 nm, respectively. The time-dependent concentration of the product pNP was calculated from the absorbance at  $\lambda = 401$  nm and the calibration curve of standard pNP.

**Tryptic Digestion of Standard Proteins and Skim Milk.** One milligram of  $\beta$ -casein or BSA was dissolved in 1 mL of NH<sub>4</sub>HCO<sub>3</sub> buffer solution (10 mM, pH 8.0), denatured at 100 °C for 5 min, and then incubated with trypsin at an enzyme-to-substrate ratio of 1:40 (w/w) at 37 °C for 16 h. For the complex sample, 30 μL of skim milk (protein content of 3.5 wt %, MUH, Germany) was added to 900 μL of NH<sub>4</sub>HCO<sub>3</sub> buffer solution (10 mM, pH 8.0) and centrifuged at 16000 rpm for 15 min. After denaturation at 100 °C for 5 min, the supernatant was mixed with 30 μg of trypsin for digestion at 37 °C for 16 h and then diluted 25-fold with the loading buffer 6% (v/v) TFA in 50% (v/v) ACN.

**Enrichment and Dephosphorylation of Phosphopeptides by MC-TiNbNS.** Digests for phosphopeptide capture were diluted with 6% (v/v) TFA in 50% (v/v) ACN. MC-TiNbNS (0.1 mg) was mixed with 200 μL of tryptic digests in an Eppendorf tube and incubated for 1 h at room temperature with gentle shaking. After being washed three times with 0.1% (v/v) TFA in 50% (v/v) ACN, the trapped phosphopeptides were dephosphorylated and eluted by 10 μL 10% NH<sub>3</sub>·H<sub>2</sub>O under sonication for 15 min. An external magnet was used for the separation and recovery of magnetic probes all through this procedure.

Human serum samples were collected from 20 healthy volunteers in Nanjing University Hospital according to the standard clinical procedures, mixed together, and stored at -80 °C before use. Typically, 10 μL of the pooled human serum was diluted by 200 μL of loading buffer 1% (v/v) TFA in water and then incubated with 0.1 mg of MC-TiNbNS in the procedure elucidated above for phosphopeptide capture and dephosphorylation.

**Apparatus.** The microwave solvothermal reaction was carried out in a DISCOVER-SP microwave synthesis system (CEM, Matthews, NC). Transmission electron microscopy (TEM) images were acquired on a JEM 1011 (JEOL 2010) electron microscope at an accelerating voltage of 200 kV. Scanning electron microscopy (SEM) was performed on a Hitachi S-4800 field-emission electron microscope at an accelerating voltage of 5 kV. UV-vis spectra were recorded on a NanoDrop 2000c spectrophotometer (Thermo Scientific, Waltham, MA). XRD patterns were collected on an ARL X'TRA X-ray diffractometer using Cu K $\alpha$  radiation ( $\lambda = 0.15405$  nm). X-ray photoelectron spectroscopy (XPS) analyses were carried out on a PHI5000 VersaProbe photoelectron spectrometer (ULVAC-PHI, Kanagawa, Japan). Nitrogen adsorption-desorption isotherms were recorded on a Micromeritics ASAP 2020 M automated sorption analyzer. The samples were degassed at 100 °C for 12 h. A superconducting quantum interference device (SQUID, Quantum Design) magnetometer was used in magnetic measurements at 300 K. Inductively coupled plasma-optical emission spectrometry (ICP-OES) experiments were conducted on an Optima 5300DV system (Perkin-Elmer, Wellesley, MA).

**Matrix-Assisted Laser Desorption/Ionization Time-of-Flight Mass Spectrometry (MALDI-TOF MS) Analysis.** The eluate (0.5 μL) and DHB matrix solution [25 mg/mL DHB in 70% (v/v) ACN, 1% (v/v) H<sub>3</sub>PO<sub>4</sub>] were deposited in turn on a steel MALDI plate. MALDI-TOF MS analysis was performed in positive reflection mode on a 4800 Plus MALDI-TOF/TOF mass spectrometer (AB Sciex) with a Nd:YAG laser at 355 nm. MS spectra were collected as averages of 16 subspectra acquired from the edge bias of the DHB matrix spot with a sum of 25 laser shots per subspectrum. The same laser intensity of 5500 was applied for all analyses. The diameter of the laser spot was 50 μm, and the power of the laser pulse was estimated to be ~5 μJ at the laser intensity value of 5500.

## RESULTS AND DISCUSSION

**Characterization of Materials.** Scanning electron microscopy (SEM) and transmission electron microscopy (TEM) images of MC-TiNbNS show two types of nanoparticles with different sizes and distributions codecorated on the 2D nanostructure, featuring visible wrinkles (Figure 1). Loosely

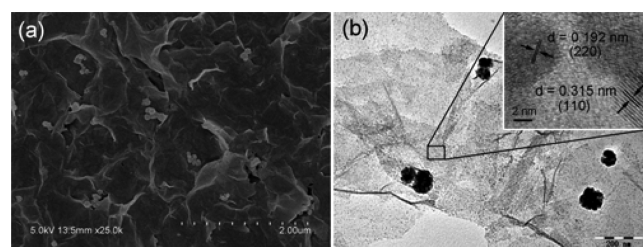


**Figure 1.** Representative (a) SEM and (b) TEM images of MC-TiNbNS. Inset: HRTEM of CeO<sub>2</sub> nanocrystals on TiNbNS.

scattered on the nanosheets is a Fe<sub>3</sub>O<sub>4</sub> polycrystalline structure with a spherical morphology sized at 60–80 nm, whereas CeO<sub>2</sub> nanoparticles with a size of 5 nm exhibit a uniform distribution all over the nanosheets (Figure 1b). The high-resolution TEM (HRTEM) image shown in the inset of Figure 1b provides information on the lattice fringes corresponding to the 111 and 220 planes of cerianite. X-ray diffraction (XRD) patterns of MC-TiNbNS show the typical diffraction peaks of CeO<sub>2</sub> and

$\text{Fe}_3\text{O}_4$ , which are indexed to JCPDS cards 04-0593 (cerianite) and 75-1610 (magnetite), respectively (Figure S1, Supporting Information), further confirming that Ce(IV) is the predominant state in cerium oxide. The predominant diffraction peak derived from the 002 plane of layered oxide  $\text{HTiNbO}_5$  was sharply passivated upon postexfoliation restacking and nanoparticle attachment, and the low-angle-shifted peak position also implied enlarged gaps between nanosheets by the foreign nanostructures of  $\text{CeO}_2$  and  $\text{Fe}_3\text{O}_4$ .

X-ray photoelectron spectroscopy (XPS) was performed to investigate the elemental composition and surface elemental valence states in the nanocomposite. The presence of all elements in the XPS survey spectrum provides solid evidence for the successful combination of all three functional parts into one nanocomposite (Figure 2a). The binding energies of Ti 2p

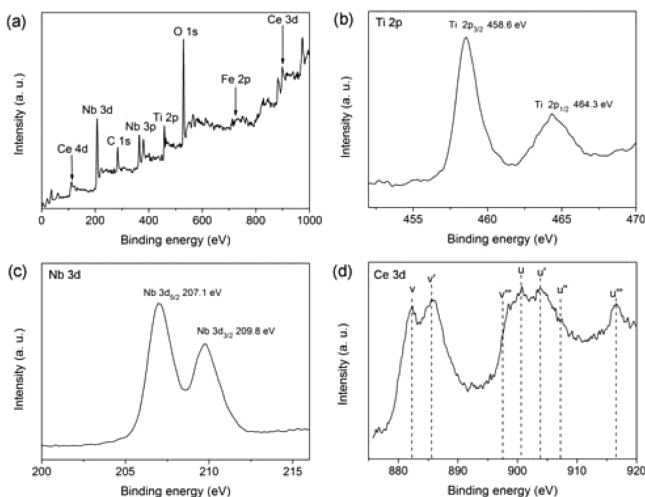


**Figure 2.** (a) XPS survey spectrum of MC-TiNbNS. (b–d) High-resolution XPS spectra of (b) Ti 2p, (c) Nb 3d, and (d) Ce 3d.

and Nb 3d are the characteristic values of Ti(IV) and Nb(V) at their highest valence states in the octahedral skeleton of the nanosheets (Figure 2b,c).<sup>50,51</sup> In the Ce 3d spectrum (Figure 2d), the peaks centered at 882.3, 885.6, 897.4, 900.7, 903.8, 907.1, and 916.5 eV are labeled as v, v', v'', u, u', u'', and u''', respectively. Doublets u'/v' and u''/v'' are derived from Ce(III) and Ce(IV), respectively, because of their characteristic photoemissions. The u/v and u''/v'' doublets are shakedown features corresponding to the transfers of one or two electrons from an occupied O 2p orbital to an empty Ce 4f orbital during

the photoemission of Ce(IV) cations.<sup>52,53</sup> Except for the characteristic peaks u''/v'' of Ce(IV), the emergence of the doublet u'/v' peaks confirmed the coexistence of Ce(III) on the oxide surface,<sup>52</sup> greatly contributing to the overall hydrolytic activity.<sup>54</sup>

Limited amounts of  $\text{Fe}_3\text{O}_4$  nanospheres were introduced to reserve as many sites as possible for  $\text{CeO}_2$  attachment under the premise of assuring flexible magnetic manipulation. Figure 3a shows that the saturation magnetization value of the ternary nanocomposite was measured to be 9.9 emu/g. Although this value was markedly decreased in comparison to that of pristine  $\text{Fe}_3\text{O}_4$  nanospheres (74.5 emu/g) because of their combination with the other two components, the composite probes could still be rapidly isolated within 1 min by use of an external magnet (Figure 3a, inset). As parts for assembling the nanocomposite,  $\text{H}^+$ -stacked TiNbNS and  $\text{CeO}_2$  nanoparticles were separately prepared as controls. Figure S2 (Supporting Information) presents the TEM images of  $\text{H}^+$ -stacked TiNbNS and  $\text{CeO}_2$  nanoparticles, the dimensions and morphologies of which appear basically identical to those in the MC-TiNbNS composite. Nitrogen adsorption–desorption experiments were carried out for MC-TiNbNS,  $\text{H}^+$ -stacked TiNbNS, and  $\text{CeO}_2$  to provide insight into the material surface structure. The Brunauer–Emmett–Teller (BET) surface area of MC-TiNbNS was calculated from the nitrogen adsorption–desorption curves to be 128.8 m<sup>2</sup>/g, larger than those of single-component  $\text{CeO}_2$  particles (66.8 m<sup>2</sup>/g) and  $\text{H}^+$ -stacked TiNbNS (33.7 m<sup>2</sup>/g), indicating that the TiNbNS 2D substrate could enhance the specific surface area of the composite accessible for guest molecules. The isotherms of both MC-TiNbNS and  $\text{H}^+$ -stacked TiNbNS were assigned to type IV isotherms with a hysteresis loop categorized as shape H3 (Figure 3b), indicative of slit-shaped mesopores formed inside aggregates of platelike nanoparticles, which reflects the disordered stacking architectures of TiNbNS. In the ternary nanocomposite, the  $\text{CeO}_2$  nanoparticles significantly contributed to the formation of a porous structure, thus giving MC-TiNbNS a higher pore distribution in the mesopore and micropore ranges than  $\text{H}^+$ -stacked TiNbNS (Figure 3c), also partially answering why the specific surface area was increased by assembling zero-dimensional  $\text{CeO}_2$  nanoparticles and magnetic beads onto 2D TiNbNS.

**Evaluation of Mimic Phosphatase Activity of MC-TiNbNS.** As a catalyst in the hydrolysis of phosphate ester bonds,  $\text{CeO}_2$  was the crucial component in the ternary nanocomposite for the final application in eliminating the phosphate moieties of phosphopeptides. Considering the

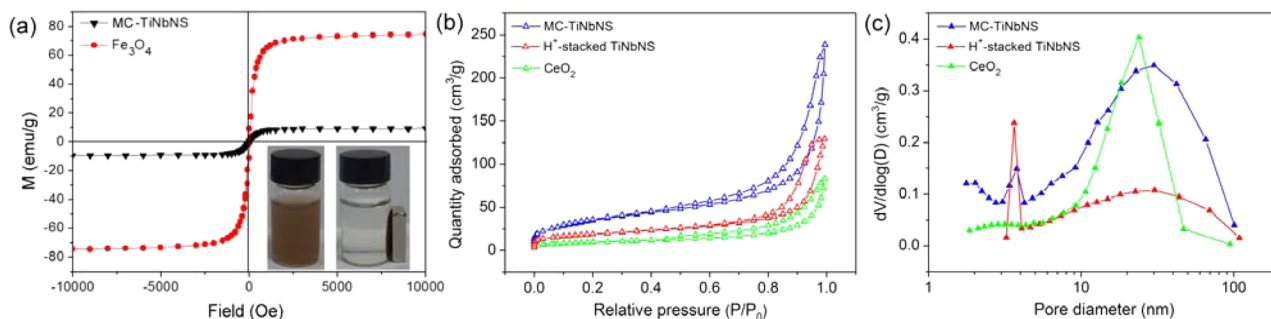


**Figure 3.** (a) Room-temperature magnetization curves of  $\text{Fe}_3\text{O}_4$  and MC-TiNbNS. Inset: Magnetic response of MC-TiNbNS to an external magnet. (b) Nitrogen adsorption–desorption curves and (c) pore distributions calculated from the desorption branches of MC-TiNbNS,  $\text{H}^+$ -stacked TiNbNS, and  $\text{CeO}_2$ .

sufficient sites for crystal growth afforded by the 2D TiNbNS platform, we attempted to adjust the catalytic activity by altering the feed ratio of the Ce source to the TiNbNS colloids. The resulting series of composites are denoted as MC-TiNbNS-*n*, where the dosage of Ce source increased with increasing value of *n* (precursor ratios are listed in Table S1, Supporting Information). Quantitative information on the Fe<sub>3</sub>O<sub>4</sub> and CeO<sub>2</sub> components in the resulting MC-TiNbNS-*n* composites was obtained by ICP-OES, and the values correlated well with the dosages of the Ce source (Table S2, Supporting Information). As shown in the TEM and SEM images recording the morphological gradient (Figure S3, Supporting Information), the compactness and dimensions of the CeO<sub>2</sub> nanoparticles were gradually raised by continuously increasing the Ce source. At the lowest precursor ratio, the CeO<sub>2</sub> nanoparticles could not be visualized even under high magnification (Figure S3a, Supporting Information); then, as the dosage of the Ce source rose, the particle size increased from 5.5 to 7.7 nm (Figure S3b–f, Supporting Information). In addition, the tiny nanocrystals were uniformly distributed on the 2D nanosheets under each set of synthetic conditions, demonstrating a high homogeneity in morphology even when the precursor ratios were varied from sample to sample. The model molecule *p*-nitrophenylphosphate (pNPP) was used to rate the catalytic activities of the MC-TiNbNS-*n* composites. Figure 4a presents UV-vis spectra of the reagent–product

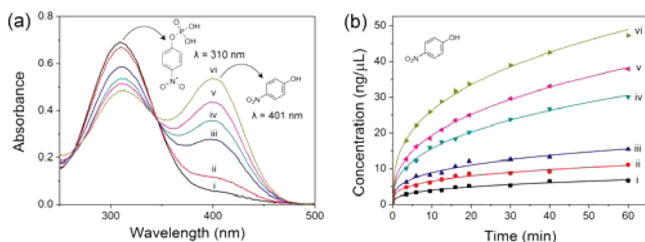


**Figure 4.** (a) UV-vis spectra of the hydrolysis product of pNPP after reacting with MC-TiNbNS-*n* for 20 min. (b) Concentration of the product pNP varying with time in the presence of MC-TiNbNS-*n*. Curves i–vi correspond to *n* values of 1–6, respectively.

couple under catalysis of MC-TiNbNS-*n* composites with different CeO<sub>2</sub> contents. At a given reaction time, the absorbance of hydrolysis product *p*-nitrophenol (pNP) regularly varied with the CeO<sub>2</sub> coverage and perfectly coincided with the decay of pNPP, confirming that the overall hydrolytic reactivity was proportional to the coating amount of CeO<sub>2</sub>. Monitoring of the pNP concentration over time indicated diverse reaction rates and yields that agreed strictly with the content of CeO<sub>2</sub> (Figure 4b), meaning that the hydrolytic capability was continuously adjustable over a large range.

#### Selective Capture and Dephosphorylation of Phosphopeptides from Digests of Standard Phosphoprotein.

With easily-tailored catalytic activity in mind, we utilized tryptic digests of standard phosphoprotein  $\beta$ -casein to investigate the applicability of the MC-TiNbNS-*n* series in phosphopeptide enrichment and dephosphorylation. After treatment with the composites with different precursor ratios, phosphopeptides and dephosphorylated species were detected in MALDI-TOF MS spectra with a clean background, and the relative ion intensity ratio of the dephosphorylated peptides to the parent phosphopeptides was found to progressively increase from 5% to 100% (Figure 5a–f), indicating that the dephosphorylation

degree could also be rationally programmed by tuning the CeO<sub>2</sub> content. Detailed peptide information is provided in Table S3 (Supporting Information).

To clarify the contributions of the three components to the extraction and dephosphorylation of phosphopeptides, Fe<sub>3</sub>O<sub>4</sub> nanospheres and CeO<sub>2</sub>-decorated TiNbNS (C-TiNbNS) were separated and employed for the selective adsorption of phosphopeptides. The Fe<sub>3</sub>O<sub>4</sub> nanospheres gave fairly weak ion signals of three phosphopeptides from digests of  $\beta$ -casein (Figure S4a, Supporting Information), whereas C-TiNbNS exhibited almost the same behavior as MC-TiNbNS in the MS peak distribution of both phosphopeptides and their dephosphorylation products (Figure S4b,c, Supporting Information), verifying that the magnetic Fe<sub>3</sub>O<sub>4</sub> component contributed little to phosphopeptide enrichment. To further demonstrate the complementary roles of TiNbNS and CeO<sub>2</sub>, the performances of individual H<sup>+</sup>-stacked TiNbNS and CeO<sub>2</sub> were assessed as well (Figure 5g,h). After the enrichment by H<sup>+</sup>-stacked TiNbNS, intense peaks from the phosphopeptides were detected, with higher sensitivity than those obtained from its precursors, namely, commercial TiO<sub>2</sub> and Nb<sub>2</sub>O<sub>5</sub> (Figure S5, Supporting Information). However, the deficiency of H<sup>+</sup>-stacked TiNbNS was its inability to offer marking signals for phosphopeptide verification, indicating that TiNbNS itself is an ideal probe for capturing phosphopeptides but is unable to mediate dephosphorylation. In the case of CeO<sub>2</sub>, the spectrum exhibited only thoroughly dephosphorylated products, from which one cannot accurately deduce the number of phosphorylation sites. Also, CeO<sub>2</sub> probes suffered relatively low sensitivity toward phosphopeptides compared to TiNbNS. In turn, by integrating the properties of TiNbNS and CeO<sub>2</sub> into one unit, the MC-TiNbNS composite ensured high sensitivity while executing the dephosphorylation in control. Note that, in any single spectrum, only some of the theoretical peaks originating from tetraphosphorylated peptide  $\beta$ 4 were detected (Table S3, Supporting Information), as also found for the strategies based on fixed-component CeO<sub>2</sub> (four peaks),<sup>24</sup> REPO<sub>4</sub> (four peaks),<sup>30,31</sup> and GdF<sub>3</sub> (three peaks).<sup>32</sup> However, by combining the spectra obtained from the series, the number of phosphorylation sites could be readily counted from the five total peaks corresponding to  $\beta$ 4. Meanwhile, because of the poor ionization efficiency of multiphosphopeptides, the low-abundance tetraphosphorylated peptide  $\beta$ 3 has rarely been reported in previous works on MOAC-based enrichment and dephosphorylation<sup>24,30,32,33,55</sup> and was undetectable at low CeO<sub>2</sub> contents in our experiments (Figure 5a,b). However, the signal of dephosphorylated  $\beta$ 3 appeared in the spectra after the Ce dosage had been increased (Figure 5e,f). In this sense, the series of component-adjustable MC-TiNbNS composites provides a global perspective on phosphorylation sites and better detection of low-abundance phosphopeptides that might be missed in simple enrichment and dephospho labeling by fixed-component materials.

**Assessment of Sensitivity, Selectivity, and Reusability.** In addition to catalytic capability, detection sensitivity was investigated using the typical composite MC-TiNbNS-3, which revealed the most dephosphorylated species and provided unbiased signals between the parent and product peptides for digests of  $\beta$ -casein (Figure 5c). MALDI-TOF MS spectra of the resulting phosphopeptides from the digests with concentration ranging from  $8 \times 10^{-8}$  to  $2 \times 10^{-10}$  M are presented in Figure S6 (Supporting Information). Phosphopeptides  $\beta$ 1,  $\beta$ 2, and  $\beta$ 4 and their dephosphorylated signatures were distinctly observed

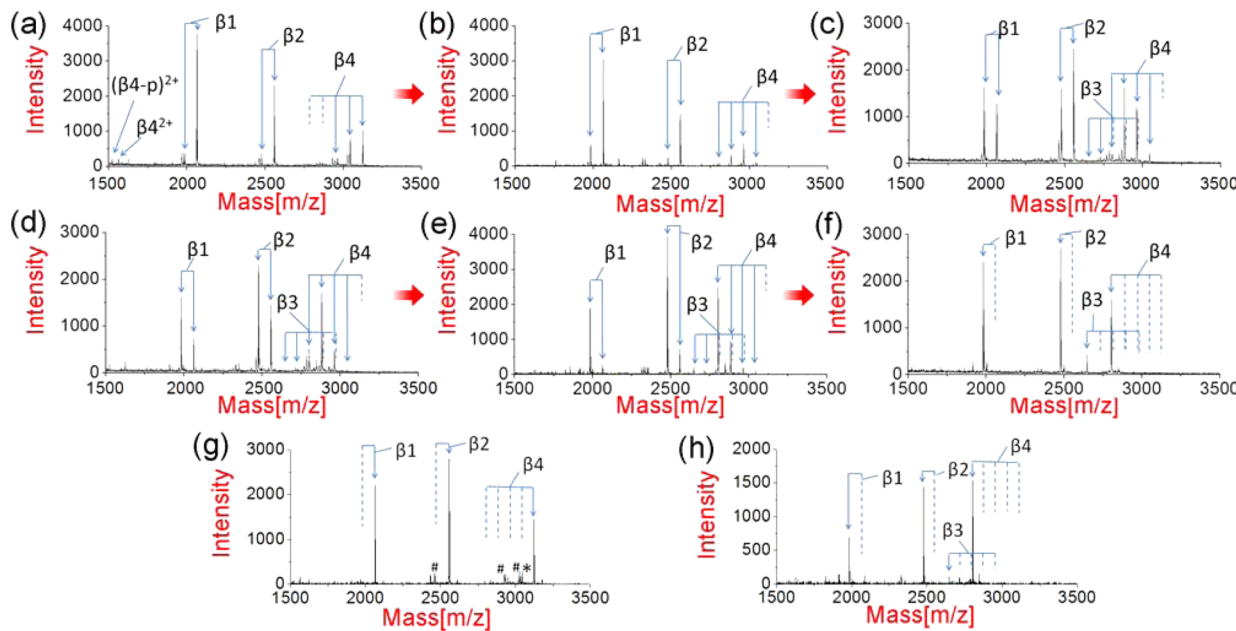


**Figure 5.** MALDI-TOF MS spectra of tryptic digests of  $\beta$ -casein ( $8 \times 10^{-8}$  M) after treatment with (a–f) MC-TiNbNS- $n$ , (g)  $H^+$ -stacked TiNbNS, and (h)  $CeO_2$ . Panels a–f correspond to  $n$  values of 1–6, respectively. Pound signs (#) and asterisks (\*) denote the neutral losses of  $H_3PO_4$  and  $HPO_3$ , respectively, from phosphopeptides upon ionization.

when the concentration dropped to  $8 \times 10^{-10}$  M (Figure S6c, Supporting Information). For an even lower concentration of  $2 \times 10^{-10}$  M, peaks belonging to  $\beta_2$  and  $\beta_4$  were still detectable with a signal-to-noise ratio of around 10 (Figure S6e, Supporting Information). With the decrease of the target phosphopeptide concentration, we found that the dephosphorylated species was correspondingly suppressed. This tendency should be due to the priority of the TiNbNS component in capturing phosphopeptides, which reduced the opportunity for dephosphorylation occurring on  $CeO_2$  component once the phosphopeptide loading was low enough.

Regarding a separation probe for extracting phosphopeptides from complex pools of biological molecules, selectivity is a critical index for judging its applicability. Here, we inspected the selectivity of MC-TiNbNS toward phosphopeptides by introducing excess digests of BSA, a nonphosphorylated protein, into digests of  $\beta$ -casein. As the mass ratio of  $\beta$ -casein to BSA was decreased from 1:10 to 1:200, the three phosphopeptides  $\beta_1$ ,  $\beta_2$ , and  $\beta_4$  were definitely identified along with their dephosphorylation clusters in the spectra (Figure S7a–d, Supporting Information), with only several weak ion signals due to the nonspecific adsorption of BSA fragments. Further addition of digests of BSA magnified the contaminant signals over those of the phosphopeptides, but the phosphopeptides with few dephosphorylated products could still be detected even at a  $\beta$ -casein-to-BSA mass ratio of 1:2000 (Figure S7e–g, Supporting Information).

Compared with other titanium-based nanomaterials proposed for phosphopeptide enrichment (for which reports in the literature on titanium-based nanostructures for extracting phosphopeptides from the past five years are listed in Table S4 of the Supporting Information), MC-TiNbNS exhibits top-middle performance on sensitivity and selectivity for phosphopeptide extraction and detection. Admittedly, owing to the differences in morphology and surface properties, MC-TiNbNS is not as effective as mesoporous  $TiO_2$ <sup>22,25</sup> polymer brush-supported  $Ti^{4+}$ -IMAC,<sup>56</sup> and some graphene-based

nanocomposites<sup>18,57,58</sup> in phosphopeptide extraction, but the ceria-decorated 2D TiNbNS nanoprobe is endowed with exceptional properties in regulating dephospho-labeling signals for phosphopeptide identification. On the other hand, among the dephospho-affinity probes (e.g., rare earth element compounds) summarized in Table S5 (Supporting Information), MC-TiNbNS displays superior sensitivity and selectivity to other probes, because of the excellent ability of the additional TiNbNS component to capture phosphopeptides. In addition to the dephospho-labeling signals for the verification of the phosphopeptides, the most significant advantage of this component-tunable composite series is its ability to produce all dephosphorylation states of each phosphopeptide, thus directly outputting a precise count of phosphorylation sites at the MS1 level, which cannot be achieved using routine cerium- or lanthanide-containing materials.<sup>24,30–32,55</sup>

Finally, the reusability of MC-TiNbNS composites was investigated using digests of  $\beta$ -casein as the analyte (Figure S8, Supporting Information). Typically, phosphopeptides from  $\beta$ -casein with a stable MS signal intensity were obtained by recycling MC-TiNbNS-3 even for four times, indicating that the phosphate affinity of the TiNbNS component remained constant during four cycles of reuse. However, the yield of dephosphorylation products decreased dramatically with the number of recycles, especially after the first use, which was also observed for other dephospho-affinity probes.<sup>30</sup> This inactivation was most likely because the phosphate moieties dissociated from phosphopeptides were still tightly attached to the active sites on the  $CeO_2$  surface, leading to the reduced catalytic activity in the following reuses.<sup>54</sup>

**Identification of Phosphopeptides from Real Samples Using MC-TiNbNS Composite.** Having confirmed the good detection sensitivity and selectivity exclusive to phosphopeptides even in the presence of high-abundance nonphosphorylated proteins of the MC-TiNbNS composite, we explored the feasibility of using this composite in capturing phosphopeptides

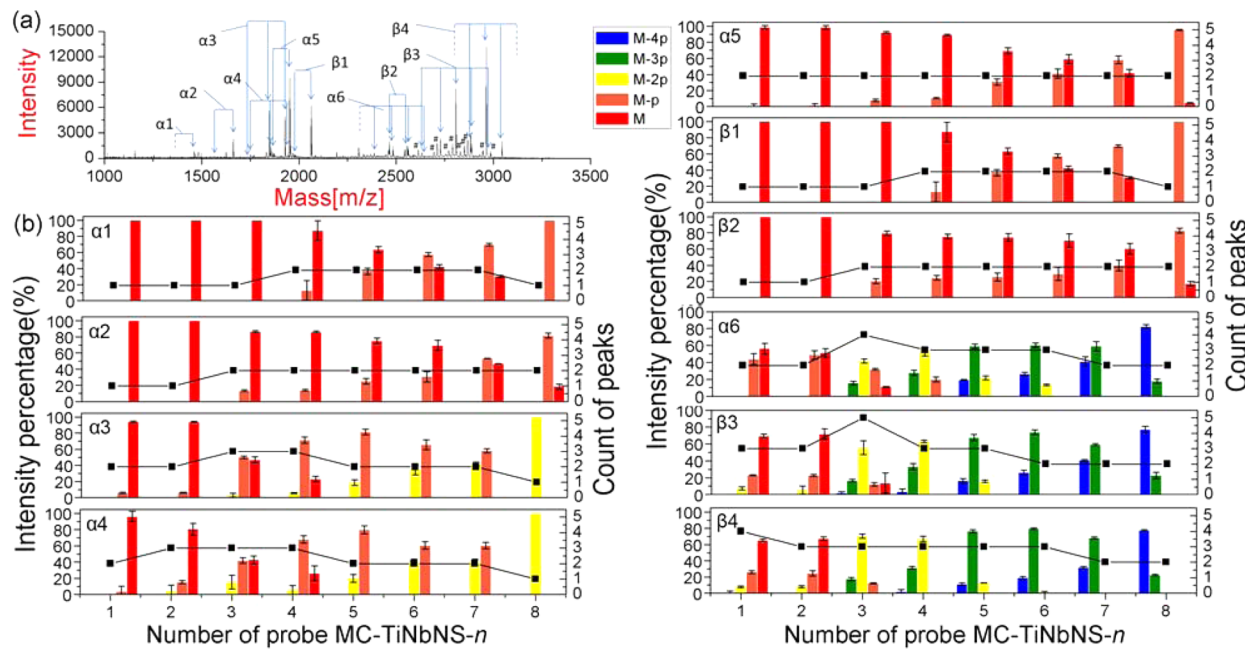


**Figure 6.** (a) Representative MALDI-TOF MS spectrum of tryptic digests of skim milk after treatment with MC-TiNbNS-3. Pound sign (#) denotes the neutral loss of  $\text{H}_3\text{PO}_4$  from the phosphopeptides upon ionization. (b) Statistics of dephosphorylation states of all 10 phosphopeptides obtained after sample preparation based on eight types of MC-TiNbNS-*n* probes (*n* = 1–8). Bar charts describe the signal intensity percentages of each dephosphorylated species normalized by the sum of all peaks belonging to the same phosphopeptide. Line graphs count the MS peaks coming from certain phosphopeptides obtained using probe MC-TiNbNS-*n*. M and M-*mp* (*m* = 1–4) symbolize the corresponding phosphopeptides and *m*-site dephosphorylation products, respectively.

from digests of skim bovine milk, a more complex sample containing casein proteins (phosphorylated proteins, such as  $\alpha$ -,  $\beta$ -, and  $\kappa$ -casein), whey proteins (nonphosphorylated proteins, such as lactoglobulin), and a number of carbohydrates. From the representative MS spectrum obtained after pretreatment with MC-TiNbNS-3 (Figure 6a), we grouped the ion signals into 10 phosphopeptides (6 from  $\alpha$ -casein and 4 from  $\beta$ -casein) marked with their graded dephosphorylation states. The sequences and masses of the identified phosphopeptides are reported in Table S6 (Supporting Information). To test the catalytic tunability, the whole series of MC-TiNbNS composites loaded with different amounts of  $\text{CeO}_2$  were used in this real case (Figure S9, Supporting Information). Unlike for standard  $\beta$ -casein, whose degraded phosphopeptides underwent complete dephosphorylation when exposed to MC-TiNbNS-6, the hydrolysis process was slightly alleviated by the biological complexity of the milk sample. To acquire a higher dephosphorylation degree, MC-TiNbNS-7 and MC-TiNbNS-8, carrying more catalytic particles, were prepared and added to the series. Figure 6b shows the dephosphorylation efficacy of the MC-TiNbNS composite from the viewpoint of each fixed phosphopeptide. In general, the proportion of dephosphorylated species was increased stepwise in contrast to the downward trend in the intensities of the pristine phosphopeptides, confirming that the functionality of the MC-TiNbNS composite in programmed dephosphorylation remained valid in the complex environment. Another observation was that the composite probes with the lowest and highest  $\text{CeO}_2$  loadings (*n* = 1 and 8) both provided fewer peaks than those with medium Ce dosages, which would maintain as many dephospho labels as possible for directly counting the phosphorylation sites from the MS1 spectrum. More convincingly, for diphosphorylated peptides  $\alpha_3$  and  $\alpha_4$  and tetraphosphorylated peptides  $\alpha_6$ ,  $\beta_3$ , and  $\beta_4$ , the most signature peaks were obtained when moderate

$\text{CeO}_2$  coverages (*n* = 3 or 4) were applied. Compared to the previously reported  $\text{Fe}_3\text{O}_4@\text{SiO}_2@\text{mCeO}_2$  (seven phosphopeptides)<sup>24</sup> and core–shell-structured  $\text{Fe}_3\text{O}_4@\text{LnPO}_4$  (five phosphopeptides),<sup>30</sup> the proposed MC-TiNbNS 2D nanoprobe captured more phosphopeptides (10 phosphopeptides) from the digests of skim milk, as well as their informative dephosphorylation products. Another recently presented ceria-based nanocomposite ( $\text{CeO}_2-\text{SnO}_2$  and  $\text{CeO}_2-\text{Fe}_2\text{O}_3$ ) selectively collected more phosphopeptides (17 phosphopeptides) than our nanoprobe, but no information on dephosphorylation fragments was obtained in that case, because of the intense phosphopeptide signals and relatively low dephosphorylation rates.<sup>33</sup> In our case, by continuously modulating the catalytic activity of the MC-TiNbNS composite, we were able to trap phosphopeptides of various abundances and phosphorylation states from a real system while labeling them and counting the modification sites by dephospho-signal clusters.

Including hundreds of proteins of high dynamic range, human serum was employed in this work as the application object to estimate the performance of MC-TiNbNS in enriching phosphopeptides from a raw biological sample. As shown by the representative MS spectrum in Figure 7a, eight peaks were clearly observed and grouped into four pairs corresponding to phosphorylated fibrinogen peptide A (FPA) and its isoforms in serum. (Peptide sequences and masses are summarized in Table S7, Supporting Information.) In addition to the signals of endogenous phosphopeptides also provided by other documented ceria-based materials,<sup>31,33,35</sup> MC-TiNbNS was capable of producing global and adjustable signals of the dephosphorylation species. As shown in Figure S10 (Supporting Information), the MS spectra displayed diverse intensity distributions of phosphopeptides versus dephospho labels, after application of the MC-TiNbNS composites with different ratios of  $\text{CeO}_2$ . Figure 7b illustrates the tradeoff between

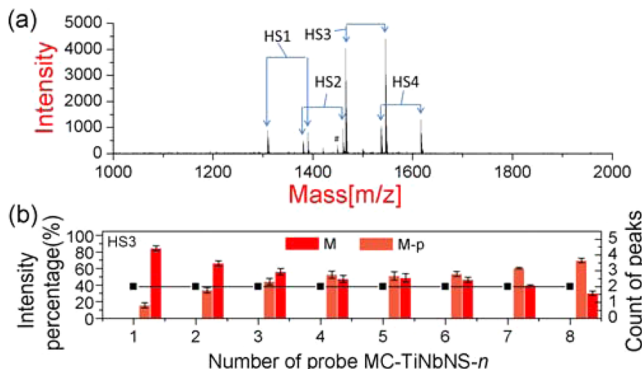


**Figure 7.** (a) Representative MALDI-TOF MS spectrum of pooled human serum after treatment with MC-TiNbNS-4. Pound sign (#) denotes the neutral loss of  $\text{H}_3\text{PO}_4$  from phosphopeptides upon ionization. (b) Statistics of dephosphorylation states of phosphopeptide HS3 obtained after sample preparation based on eight types of MC-TiNbNS-*n* probes (*n* = 1–8). The bar chart describes the signal intensity percentages of each dephosphorylated species normalized by the sum of all peaks derived from HS3. The line graph counts all of the MS peaks assigned to HS3 obtained using probe MC-TiNbNS-*n*. M and M-p symbolize the intact phosphopeptide HS3 and the single-site dephosphorylation product.

phosphopeptide HS3 and its dephosphorylation marker, whose intensities monotonically decreased and increased, respectively, with variations in the  $\text{CeO}_2$  loading, demonstrating the ability of the MC-TiNbNS composite to control the hydrolysis of the phosphate ester bonds of phosphopeptides under conditions of overwhelming biological molecules. By monitoring its application behaviors in skim milk and human serum, we confirmed the feasibility of the MC-TiNbNS composites to capture and identify phosphopeptides from real biological samples. More importantly, the complete readout of all dephosphorylated species indicated that, even for biological cases, comprehensive characterization of the phosphorylation sites under MS1 conditions can still be realized by continuously adjusting the  $\text{CeO}_2$  coverage in the MC-TiNbNS series.

## CONCLUSIONS

To summarize, a 2D ternary composite MC-TiNbNS combining magnetic separability, phosphate affinity, and adjustable dephosphorylation activity was prepared by preloading of  $\text{Fe}_3\text{O}_4$  followed by in situ growth of  $\text{CeO}_2$  on TiNbNS and then applied to phosphopeptide enrichment and programmed dephosphorylation. The MS signals of the parent phosphopeptides and each dephosphorylation signature were simultaneously detected and flexibly regulated by tuning the  $\text{CeO}_2$  coverage on TiNbNS. With remarkable detection sensitivity and selectivity to phosphopeptides, this composite probe series can also provide exhaustive information on low-abundance multiphosphopeptides and phosphorylation site counts. This unique property in both capturing and labeling phosphopeptides still remained reliable in skim milk and human serum specimens because of the good tolerance of the composite to high biological complexity. Our study opens a universal pathway for the highly efficient extraction and global identification of both mono- and multiphosphopeptides with accurate site counting at the MS1 level and highlights the potential of 2D multicomponent composites for functional integration in various applications.

## ASSOCIATED CONTENT

### Supporting Information

Precursor ratios for the synthesis of MC-TiNbNS; mass fractions of  $\text{Fe}_3\text{O}_4$  and  $\text{CeO}_2$  in MC-TiNbNS-*n*; phosphopeptides and dephosphorylation products identified from digests of  $\beta$ -casein, skim milk, and human serum; literature on the enrichment of phosphopeptides by nanomaterials; supplementary characterizations of MC-TiNbNS; sensitivity, selectivity, and reusability of MC-TiNbNS composite toward phosphopeptides; MALDI-TOF MS spectra of tryptic digests of skim milk and raw serum treated by MC-TiNbNS with different  $\text{CeO}_2$  coverages. This material is available free of charge via the Internet at <http://pubs.acs.org>.

## AUTHOR INFORMATION

### Corresponding Authors

\*E-mail: jianglp@nju.edu.cn. Tel./Fax: +86-25-8359-7204.

\*E-mail: jjzhu@nju.edu.cn. Tel./Fax: +86-25-8359-7204.

### Author Contributions

<sup>‡</sup>Q.M. and S.L. contributed equally to this work.

### Notes

The authors declare no competing financial interest.

## ACKNOWLEDGMENTS

This research was financially supported by the National Basic Research Program of China (2011CB933502), the National Natural Science Foundation of China (21205060, 21335004), and the Research Fund for the Doctoral Program of Higher Education of China (20120091120029). This work was also supported by the Program for New Century Excellent Talents in University (NCET-12-0256). The authors extend their appreciation to the Deanship of Scientific Research at King Saud University for funding this work through International Research Group Project RGP-VPP-029.

## REFERENCES

- Olsen, J. V.; Blagoev, B.; Gnad, F.; Macek, B.; Kumar, C.; Mortensen, P.; Mann, M. Global, In Vivo, and Site-Specific Phosphorylation Dynamics in Signaling Networks. *Cell* **2006**, *127*, 635–48.
- Aebersold, R.; Mann, M. Mass Spectrometry-Based Proteomics. *Nature* **2003**, *422*, 198.
- Zhou, H.; Watts, J. D.; Aebersold, R. A Systematic Approach to the Analysis of Protein Phosphorylation. *Nat. Biotechnol.* **2001**, *19*, 375.
- Kalume, D. E.; Molina, H.; Pandey, A. Tackling the Phosphoproteome: Tools and Strategies. *Curr. Opin. Chem. Biol.* **2003**, *7*, 64–69.
- Knight, Z. A.; Schilling, B.; Row, R. H.; Kenski, D. M.; Gibson, B. W.; Shokat, K. M. Phosphospecific Proteolysis for Mapping Sites of Protein Phosphorylation. *Nat. Biotechnol.* **2003**, *21*, 1047–1054.
- Ficarro, S. B.; McCleland, M. L.; Stukenberg, P. T.; Burke, D. J.; Ross, M. M.; Shabanowitz, J.; Hunt, D. F.; White, F. M. Phosphoproteome Analysis by Mass Spectrometry and Its Application to *Saccharomyces cerevisiae*. *Nat. Biotechnol.* **2002**, *20*, 301–305.
- Posewitz, M. C.; Tempst, P. Immobilized Gallium(III) Affinity Chromatography of Phosphopeptides. *Anal. Chem.* **1999**, *71*, 2883–2892.
- Nuhse, T. S.; Stensballe, A.; Jensen, O. N.; Peck, S. C. Large-Scale Analysis of In Vivo Phosphorylated Membrane Proteins by Immobilized Metal Ion Affinity Chromatography and Mass Spectrometry. *Mol. Cell. Proteomics* **2003**, *2*, 1234–1243.
- Larsen, M. R.; Thingholm, T. E.; Jensen, O. N.; Roepstorff, P.; Jorgensen, T. J. D. Highly Selective Enrichment of Phosphorylated

- Peptides from Peptide Mixtures Using Titanium Dioxide Microcolumns. *Mol. Cell. Proteomics* **2005**, *4*, 873–886.
- (10) Kweon, H. K.; Hakansson, K. Selective Zirconium Dioxide-Based Enrichment of Phosphorylated Peptides for Mass Spectrometric Analysis. *Anal. Chem.* **2006**, *78*, 1743–1749.
- (11) Pinkse, M. W. H.; Uitto, P. M.; Hilhorst, M. J.; Ooms, B.; Heck, A. J. R. Selective Isolation at the Femtomole Level of Phosphopeptides from Proteolytic Digests Using 2D-NanoLC-ESI-MS/MS and Titanium Oxide Precolumns. *Anal. Chem.* **2004**, *76*, 3935–3943.
- (12) Thingholm, T. E.; Jorgensen, T. J. D.; Jensen, O. N.; Larsen, M. R. Highly Selective Enrichment of Phosphorylated Peptides Using Titanium Dioxide. *Nat. Protoc.* **2006**, *1*, 1929–1935.
- (13) Zhou, H.; Tian, R.; Ye, M.; Xu, S.; Feng, S.; Pan, C.; Jiang, X.; Li, X.; Zou, H. Highly Specific Enrichment of Phosphopeptides by Zirconium Dioxide Nanoparticles for Phosphoproteome Analysis. *Electrophoresis* **2007**, *28*, 2201–2215.
- (14) Lu, J.; Liu, S.; Deng, C. Facile Synthesis of Alumina Hollow Spheres for On-Plate-Selective Enrichment of Phosphopeptides. *Chem. Commun.* **2011**, *47*, 5334–5336.
- (15) Qiao, L.; Bi, H.; Busnel, J.-M.; Hojeij, M.; Mendez, M.; Liu, B.; Girault, H. H. Controlling the Specific Enrichment of Multi-Phosphorylated Peptides on Oxide Materials: Aluminium Foil as a Target Plate for Laser Desorption Ionization Mass Spectrometry. *Chem. Sci.* **2010**, *1*, 374–382.
- (16) Ficarro, S. B.; Parikh, J. R.; Blank, N. C.; Marto, J. A. Niobium(V) Oxide ( $\text{Nb}_2\text{O}_5$ ): Application to Phosphoproteomics. *Anal. Chem.* **2008**, *80*, 4606–4613.
- (17) Qi, D.; Lu, J.; Deng, C.; Zhang, X. Magnetically Responsive  $\text{Fe}_3\text{O}_4@\text{C}@\text{SnO}_2$  Core–Shell Microspheres: Synthesis, Characterization, and Application in Phosphoproteomics. *J. Phys. Chem. C* **2009**, *113*, 15854–15861.
- (18) Wang, M.; Deng, C.; Li, Y.; Zhang, X. Magnetic Binary Metal Oxides Affinity Probe for Highly Selective Enrichment of Phosphopeptides. *ACS Appl. Mater. Interfaces* **2014**, *6*, 11775–11782.
- (19) Lu, Z.; Duan, J.; He, L.; Hu, Y.; Yin, Y. Mesoporous  $\text{TiO}_2$  Nanocrystal Clusters for Selective Enrichment of Phosphopeptides. *Anal. Chem.* **2010**, *82*, 7249–7258.
- (20) Nelson, C. A.; Szczech, J. R.; Xu, Q.; Lawrence, M. J.; Jin, S.; Ge, Y. Mesoporous Zirconium Oxide Nanomaterials Effectively Enrich Phosphopeptides for Mass Spectrometry-Based Phosphoproteomics. *Chem. Commun.* **2009**, *43*, 6607–6609.
- (21) Li, L.; Chen, S.; Xu, L.; Bai, Y.; Nie, Z.; Liu, H.; Qi, L. Template-Free Synthesis of Uniform Mesoporous  $\text{SnO}_2$  Nanospheres for Efficient Phosphopeptide Enrichment. *J. Mater. Chem. B* **2014**, *2*, 1121–1124.
- (22) Yan, Y.; Zhang, X.; Deng, C. Designed Synthesis of Titania Nanoparticles Coated Hierarchically Ordered Macro/Mesoporous Silica for Selective Enrichment of Phosphopeptides. *ACS Appl. Mater. Interfaces* **2014**, *6*, 5467–5471.
- (23) Li, X.-S.; Pan, Y.-N.; Zhao, Y.; Yuan, B.-F.; Guo, L.; Feng, Y.-Q. Preparation of Titanium-Grafted Magnetic Mesoporous Silica for the Enrichment of Endogenous Serum Phosphopeptides. *J. Chromatogr. A* **2013**, *1315*, 61–69.
- (24) Cheng, G.; Zhang, J.-L.; Liu, Y.-L.; Sun, D.-H.; Ni, J.-Z. Synthesis of Novel  $\text{Fe}_3\text{O}_4@\text{SiO}_2@\text{CeO}_2$  Microspheres with Mesoporous Shell for Phosphopeptide Capturing and Labeling. *Chem. Commun.* **2011**, *47*, 5732–5734.
- (25) Ma, W.-F.; Zhang, Y.; Li, L.-L.; You, L.-J.; Zhang, P.; Zhang, Y.-T.; Li, J.-M.; Yu, M.; Guo, J.; Lu, H.-J.; Wang, C.-C. Tailor-Made Magnetic  $\text{Fe}_3\text{O}_4@m\text{TiO}_2$  Microspheres with a Tunable Mesoporous Anatase Shell for Highly Selective and Effective Enrichment of Phosphopeptides. *ACS Nano* **2012**, *6*, 3179–3188.
- (26) Li, Y.; Zhang, X.; Deng, C. Functionalized Magnetic Nanoparticles for Sample Preparation in Proteomics and Peptidomics Analysis. *Chem. Soc. Rev.* **2013**, *42*, 8517–8539.
- (27) Li, X.-S.; Zhu, G.-T.; Luo, Y.-B.; Yuan, B.-F.; Feng, Y.-Q. Synthesis and Applications of Functionalized Magnetic Materials in Sample Preparation. *TrAC, Trends Anal. Chem.* **2013**, *45*, 233–247.
- (28) Tan, F.; Zhang, Y.; Wang, J.; Wei, J.; Cai, Y.; Qian, X. An Efficient Method for Dephosphorylation of Phosphopeptides by Cerium Oxide. *J. Mass Spectrom.* **2008**, *43*, 628–632.
- (29) Wu, J.-H.; Xiao, K.; Zhao, Y.; Zhang, W.-P.; Guo, L.; Feng, Y.-Q. Preparation and Characterization of Ceria–Zirconia Composite for Enrichment and Identification of Phosphopeptides. *J. Sep. Sci.* **2010**, *33*, 2361–2368.
- (30) Wang, Z.-G.; Cheng, G.; Liu, Y.-L.; Zhang, J.-L.; Sun, D.-H.; Ni, J.-Z. Fabrication of Novel Hierarchical Structured  $\text{Fe}_3\text{O}_4@\text{LnPO}_4$  ( $\text{Ln} = \text{Eu}$ ,  $\text{Tb}$ ,  $\text{Er}$ ) Multifunctional Microspheres for Capturing and Labeling Phosphopeptides. *Small* **2012**, *8*, 3456–3464.
- (31) Cheng, G.; Zhang, J.-L.; Liu, Y.-L.; Sun, D.-H.; Ni, J.-Z. Monodisperse REPO<sub>4</sub> (RE = Yb, Gd, Y) Hollow Microspheres Covered with Nanothorns as Affinity Probes for Selectively Capturing and Labeling Phosphopeptides. *Chem.—Eur. J.* **2012**, *18*, 2014–2020.
- (32) Li, L.-P.; Liu, J.-Z.; Xu, L.-N.; Li, Z.; Bai, Y.; Xiao, Y.-L.; Liu, H.-W.  $\text{GdF}_3$  as a Promising Phosphopeptide Affinity Probe and Dephospho-Labelling Medium: Experiments and Theoretical Explanation. *Chem. Commun.* **2014**, *50*, 11572–11575.
- (33) Fatima, B.; Najam-ul-Haq, M.; Jabeen, F.; Majeed, S.; Ashiq, M. N.; Musharraf, S. G.; Shad, B. A.; Xu, G. Ceria-Based Nanocomposites for the Enrichment and Identification of Phosphopeptides. *Analyst* **2013**, *138*, 5059–5067.
- (34) Nelson, C. A.; Szczech, J. R.; Dooley, C. J.; Xu, Q.; Lawrence, M. J.; Zhu, H.; Jin, S.; Ge, Y. Effective Enrichment and Mass Spectrometry Analysis of Phosphopeptides Using Mesoporous Metal Oxide Nanomaterials. *Anal. Chem.* **2010**, *82*, 7193–7201.
- (35) Wu, J.-H.; Li, X.-S.; Zhao, Y.; Gao, Q.; Guo, L.; Feng, Y.-Q. Titania Coated Magnetic Mesoporous Hollow Silica Microspheres: Fabrication and Application to Selective Enrichment of Phosphopeptides. *Chem. Commun.* **2010**, *46*, 9031–9033.
- (36) Wan, J.; Qian, K.; Qiao, L.; Wang, Y.; Kong, J.; Yang, P.; Liu, B.; Yu, C.  $\text{TiO}_2$ -Modified Macroporous Silica Foams for Advanced Enrichment of Multi-Phosphorylated Peptides. *Chem.—Eur. J.* **2009**, *15*, 2504–2508.
- (37) Min, Q.; Zhang, X.; Zhang, H.; Zhou, F.; Zhu, J.-J. Synthesis of  $\text{Fe}_3\text{O}_4$ -Graphene– $\text{TiO}_2$  Ternary Composite Networks for Enhanced Capture of Phosphopeptides. *Chem. Commun.* **2011**, *47*, 11709–11711.
- (38) Pang, H.; Lu, Q.; Gao, F. Graphene Oxide Induced Growth of One-Dimensional Fusiform Zirconia Nanostructures for Highly Selective Capture of Phosphopeptides. *Chem. Commun.* **2011**, *47*, 11772–11774.
- (39) Lu, J.; Deng, C.; Zhang, X.; Yang, P. Synthesis of  $\text{Fe}_3\text{O}_4$ /Graphene/ $\text{TiO}_2$  Composites for the Highly Selective Enrichment of Phosphopeptides from Biological Samples. *ACS Appl. Mater. Interfaces* **2013**, *5*, 7330–7334.
- (40) Zhu, Y.; Murali, S.; Cai, W.; Li, X.; Suk, J. W.; Potts, J. R.; Ruoff, R. S. Graphene and Graphene Oxide: Synthesis, Properties, and Applications. *Adv. Mater.* **2010**, *22*, 3906–3924.
- (41) Butler, S. Z.; Hollen, S. M.; Cao, L.; Cui, Y.; Gupta, J. A.; Gutierrez, H. R.; Heinz, T. F.; Hong, S. S.; Huang, J.; Ismach, A. F.; Johnston-Halperin, E.; Kuno, M.; Plashnitsa, V. V.; Robinson, R. D.; Ruoff, R. S.; Salahuddin, S.; Shan, J.; Shi, L.; Spencer, M. G.; Terrones, M.; Windl, W.; Goldberger, J. E. Progress, Challenges, and Opportunities in Two-Dimensional Materials Beyond Graphene. *ACS Nano* **2013**, *7*, 2898–2926.
- (42) Zhang, Y.; Zheng, B.; Zhu, C.; Zhang, X.; Tan, C.; Li, H.; Chen, B.; Yang, J.; Chen, J.; Huang, Y.; Wang, L.; Zhang, H. Single-Layer Transition Metal Dichalcogenide Nanosheet-Based Nanosensors for Rapid, Sensitive, and Multiplexed Detection of DNA. *Adv. Mater.* **2014**, *27*, 935–939.
- (43) Liang, S. J.; Wen, L. R.; Lin, S.; Bi, J. H.; Feng, P. Y.; Fu, X. Z.; Wu, L. Monolayer  $\text{HNb}_3\text{O}_8$  for Selective Photocatalytic Oxidation of Benzylic Alcohols with Visible Light Response. *Angew. Chem., Int. Ed.* **2014**, *53*, 2951–2955.
- (44) Huang, X.; Zeng, Z.; Zhang, H. Metal Dichalcogenide Nanosheets: Preparation, Properties and Applications. *Chem. Soc. Rev.* **2013**, *42*, 1934–1946.

- (45) Lu, J.; Wang, M. Y.; Li, Y.; Deng, C. H. Facile Synthesis of TiO<sub>2</sub>/Graphene Composites for Selective Enrichment of Phosphopeptides. *Nanoscale* **2012**, *4*, 1577–1580.
- (46) Xu, L. N.; Li, L. P.; Jin, L.; Bai, Y.; Liu, H. W. Guanidyl-Functionalized Graphene as a Bifunctional Adsorbent for Selective Enrichment of Phosphopeptides. *Chem. Commun.* **2014**, *50*, 10963–10966.
- (47) Yan, Y. H.; Zheng, Z. F.; Deng, C. H.; Li, Y.; Zhang, X. M.; Yang, P. Y. Hydrophilic Polydopamine-Coated Graphene for Metal Ion Immobilization as a Novel Immobilized Metal Ion Affinity Chromatography Platform for Phosphoproteome Analysis. *Anal. Chem.* **2013**, *85*, 8483–8487.
- (48) Cheng, G.; Wang, Z. G.; Liu, Y. L.; Zhang, J. L.; Sun, D. H.; Ni, J. Z. A Graphene-Based Multifunctional Affinity Probe for Selective Capture and Sequential Identification of Different Biomarkers from Biosamples. *Chem. Commun.* **2012**, *48*, 10240–10242.
- (49) Chen, X.; Li, S.; Zhang, X.; Min, Q.; Zhu, J.-J. Weaving a Two-Dimensional Fishing Net of Fe<sub>3</sub>O<sub>4</sub> Nanocrystals-Embedded Titanonobate Nanosheet for Highly Efficient Capture and Isotope Labeling of Phosphopeptides. *Nanoscale* **2015**, *7*, 5815–5825.
- (50) Biesinger, M. C.; Lau, L. W. M.; Gerson, A. R.; Smart, R. S. C. Resolving Surface Chemical States in XPS Analysis of First Row Transition Metals, Oxides and Hydroxides: Sc, Ti, V, Cu and Zn. *Appl. Surf. Sci.* **2010**, *257*, 887–898.
- (51) Moulder, J. F.; Stickle, W. F.; Sobol, P. E.; Bomben, K. D.; Chastain, J. *Handbook of X-ray Photoelectron Spectroscopy*; PerkinElmer: Eden Prairie, MN, 1992.
- (52) Reddy, B. M.; Khan, A.; Yamada, Y.; Kobayashi, T.; Loridan, S.; Volta, J. C. Structural Characterization of CeO<sub>2</sub>–TiO<sub>2</sub> and V<sub>2</sub>O<sub>5</sub>/CeO<sub>2</sub>–TiO<sub>2</sub> Catalysts by Raman and XPS Techniques. *J. Phys. Chem. B* **2003**, *107*, 5162–5167.
- (53) Assumpcao, M. H. M. T.; Moraes, A.; De Souza, R. F. B.; Reis, R. M.; Rocha, R. S.; Gaubeur, I.; Calegaro, M. L.; Hammer, P.; Lanza, M. R. V.; Santos, M. C. Degradation of Dipyrone via Advanced Oxidation Processes Using a Cerium Nanostructured Electrocatalyst Material. *Appl. Catal. A* **2013**, *462*, 256–261.
- (54) Kuchma, M. H.; Komanski, C. B.; Colon, J.; Teblum, A.; Masunov, A. E.; Alvarado, B.; Babu, S.; Seal, S.; Summy, J.; Baker, C. H. Phosphate Ester Hydrolysis of Biologically Relevant Molecules by Cerium Oxide Nanoparticles. *Nanomedicine (N. Y., NY, U. S.)* **2010**, *6*, 738–744.
- (55) Cheng, G.; Wang, Z.-G.; Liu, Y.-L.; Zhang, J.-L.; Sun, D.-H.; Ni, J.-Z. A Graphene-Based Multifunctional Affinity Probe for Selective Capture and Sequential Identification of Different Biomarkers from Biosamples. *Chem. Commun.* **2012**, *48*, 10240–10242.
- (56) Zhao, L.; Qin, H. Q.; Hu, Z. Y.; Zhang, Y.; Wu, R. A.; Zou, H. F. A Poly(ethylene glycol)-Brush Decorated Magnetic Polymer for Highly Specific Enrichment of Phosphopeptides. *Chem. Sci.* **2012**, *3*, 2828–2838.
- (57) Tang, L. A. L.; Wang, J.; Lim, T. K.; Bi, X.; Lee, W. C.; Lin, Q.; Chang, Y.-T.; Lim, C. T.; Loh, K. P. High-Performance Graphene-Titania Platform for Detection of Phosphopeptides in Cancer Cells. *Anal. Chem.* **2012**, *84*, 6693–6700.
- (58) Yan, Y.; Sun, X.; Deng, C.; Li, Y.; Zhang, X. Metal Oxide Affinity Chromatography Platform-Polydopamine Coupled Functional Two-Dimensional Titania Graphene Nanohybrid for Phosphoproteome Research. *Anal. Chem.* **2014**, *86*, 4327–4332.